

Article pubs.acs.org/JPCA

Electronic Spectroscopy and Photoionization of LiBe

Published as part of The Journal of Physical Chemistry virtual special issue "Daniel Neumark Festschrift".

Thomas D. Persinger, Jiande Han, and Michael C. Heaven*



Cite This: J. Phys. Chem. A 2021, 125, 8274-8281



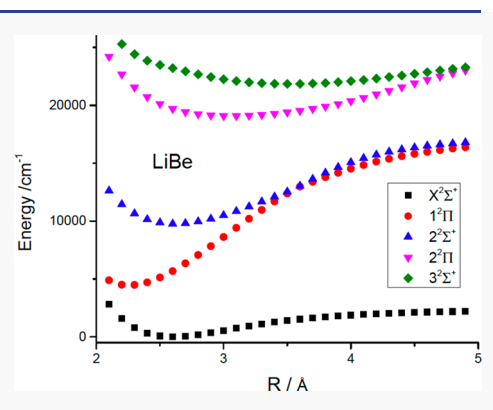
ACCESS

Metrics & More

Article Recommendations

Supporting Information

ABSTRACT: LiBe has been the subject of several theoretical investigations and one spectroscopic study. Initially, these efforts were motivated by interest in the intermetallic bond. More recent work has explored the potential for producing LiBe and LiBe+ at ultracold temperatures. In the present study, we have advanced the spectroscopic characterization of several electronic states of LiBe and the ground state of LiBe⁺. For the neutral molecule, the $1^2\Pi$, $2^2\Sigma^+$, $3^2\Sigma^+$, and $4^2\Pi(3d)$ states were observed for the first time. Data for the $2^2\Sigma^+-X^2\Sigma^+$ transition support a theoretical prediction that this band system is suitable for direct laser cooling. Photoelectron spectroscopy has been used to determine the ionization energy of LiBe and map the low-energy vibrational levels of LiBe⁺ $X^1\Sigma^+$. Overall, the results validate the predictions of high-level quantum chemistry calculations for both LiBe and LiBe+.



INTRODUCTION

LiBe, which holds the distinction of being the simplest intermetallic species, has been the subject of several theoretical studies. Although initial electronic structure calculations predicted that ground-state LiBe would not be bound, ²⁻⁴ Schlachta et al. ¹ succeeded in producing LiBe in the gas phase by the laser vaporization of a Li/Be pressed pellet. Using the laser-induced fluorescence (LIF) technique, they observed bands of the $C^2\Pi - X^2\Sigma^+$ transition within the 19 200-20 600 cm⁻¹ energy range. Multireference configuration interaction (MRCI) calculations, presented in the same paper, predicted that the ground state was bound by 2476 cm⁻¹. This magnitude was consistent with the expected halforder bond. Surprisingly, the bond length was found to be shorter than that of covalently bound Li₂ (2.59 vs 2.67 Å). Theoretical calculations indicated that the $C^2\Pi$ state was correlated to the $Li(^2S) + Be(^3P)$ dissociation asymptote (note that this state is labeled as $2^2\Pi$ in more recent literature). Lower-energy excited states $(1^2\Pi$ and $2^2\Sigma^+)$ that correlate with the $Li(^{2}P) + Be(^{1}S)$ dissociation limit were predicted, but no attempt was made to observe these states.

Subsequent theoretical calculations for LiBe have predicted properties for the ground state and a range of electronically excited states.^{8–16} A subset of this work has been motivated by the potential for cooling LiBe or the LiBe+ cation to ultracold temperatures. 12,14,16-20 From this perspective, the attractive attributes of LiBe(X) for ultracold molecule studies include a large dipole moment (predicted to be 3.5 D12,16) and the magnetic moment associated with the unpaired electron. You et al. 14 examined the possibilities for direct laser cooling of LiBe. Their MRCI calculations indicate that the $2^2\Sigma^+$ - $X^2\Sigma^+$

transition is very diagonal, with a Franck-Condon factor for the 0-0 band of 0.998 (note that SrF has been successfully laser cooled using an electronic transition that has a 0-0 band FCF of 0.98²¹). The computed electronic transition dipole moment of the $2^2\Sigma^+-X^2\Sigma^+$ transition is large, yielding an excited-state radiative lifetime of about 75 ns. These predictions suggest that laser cooling is feasible. 14

The LiBe⁺ cation is also of interest from the perspectives of bonding and cold molecular ion manipulation. The $X^1\Sigma^+$ ground state can be viewed as the interaction between the closed-shell Li⁺(¹S) and Be(¹S) moieties. Theory predicts a binding energy that is approximately a factor of 2 greater than that of neutral LiBe(X), with a permanent dipole moment (3.55 D) that is almost unchanged by ionization. 17,18,20 Cold LiBe+ could be generated by at least two paths. The first, dependent on verification that laser cooling of LiBe is feasible, would involve the photoionization of cold LiBe. The second would be to photoassociate laser-cooled Be⁺ with cold Li. This scenario has been examined by Rakshit and Deb, 19 who analyzed the photoassociation process using model potential energy curves and transition moments for the $2^{1}\Sigma^{+}-X^{1}\Sigma^{+}$ transition.

In the present study, we have extended the experimental characterization of LiBe to include the $1^2\Pi$ and $2^2\Sigma^+$ states and

Received: August 7, 2021 Published: September 14, 2021





a group of transitions in the near-UV spectral range. The ionization energy (IE) of LiBe and the vibrational structure of the ground-state LiBe⁺ ion have been examined using pulsed-field ionization—zero kinetic energy (PFI-ZEKE) photoelectron spectroscopy. This study closely parallels our recent work on LiMg/LiMg^{+, 22}

■ EXPERIMENTAL SECTION

The techniques used to characterize LiBe consisted of LIF, dispersed LIF (DLIF), resonance-enhanced two-photon ionization (RE2PI), photoionization efficiency (PIE), and PFI-ZEKE spectroscopy. ²² Gas-phase LiBe was obtained by laser ablation of the surface of a Li-coated Be rod. The Li coating was applied by rubbing samples of Li metal against the surface of the 6.35-mm-diameter Be rod. Laser ablation was achieved using 1064 nm pulses from a Nd/YAG laser. Typically, the rod could be used for about 3 days before the Li coating needed to be reapplied.

The Li-coated Be rod was mounted in a Smalley-type jet expansion source.²³ The rod was rotated and translated to avoid pitting. The carrier gas used for these experiments was pure He, supplied by a pulsed valve (Parker-Hannifin series 9) at a source pressure of 5 atm. LIF and DLIF spectra were recorded with the excitation laser beam set to cross the jet expansion approximately 7.5 cm downstream from the nozzle orifice. LIF was collected along an axis that was perpendicular to both the laser beam axis and the jet expansion axis. For the recording of LIF data, a long-pass filter was used to reduce the scattered laser light, and the filtered fluorescence was detected by a photomultiplier tube (Photonis XP2020). Fluorescence decay curves, acquired using a digital oscilloscope (LeCroy WaveSurfer 24Xs) to signal average 500 laser pulses per trace, were measured using the same setup. As scattered laser light dominated the signal during the first 20 ns, a background trace was accumulated with the ablation laser blocked. This signal was then subtracted from the fluorescence plus scatter trace. An example is shown in the Supporting Information. DLIF spectra were obtained when the long-pass filter was replaced with a 0.25 m monochromator (Jarrell-Ash 82-410).

Three tunable dye laser systems were used in these experiments. Two were Nd/YAG pumped systems, consisting of a Lambda Physik Scan Mate Pro driven by a Quantel Q-smart 850 Nd/YAG, and a Continuum ND6000 dye laser driven by a Powerlite 8000 Nd/YAG laser. The third system was a Lambda Physik FL3002 dye laser pumped by a Lextra XeCl excimer laser. In their standard configurations, all three dye lasers operated with line widths (fwhm) of approximately 0.3 cm⁻¹. For higher-resolution measurements, the line width of the FL3002 laser was reduced to 0.06 cm⁻¹ by means of an intracavity etalon. Wavelength calibration of the lasers was established using a Bristol Instruments model 821 wavemeter.

RE2PI, PIE, and PFI-ZEKE measurements were carried out in a differentially pumped vacuum chamber that was equipped for time-of-flight mass spectrometry and electron detection. RE2PI and PIE spectra were recorded with mass-resolved ion detection. RE2PI data for transitions occurring in the near-UV spectral range were obtained using one-color, two-photon ionization. This was possible because the excited-state energies were more than half of the IE. RE2PI spectra for lower energy states were observed using two-color ionization. Frequency doubling of the light from the ND6000 laser yielded wavelengths (usually near 280 nm and held constant for each scan) that could readily ionize LiBe that had been excited

to the $2^2\Pi$ or $3^2\Sigma^+$ states. Tunable laser pulses at wavelengths near 1020 nm were needed to examine the $2^2\Sigma^+ - X^2\Sigma^+$ transition. This radiation was generated by Raman shifting of the output from the ND6000 laser using H_2 . The Raman shifting cell was 1 m long and filled with H_2 to a pressure of 300 psia. A 1 m focal length lens was used to focus the dye laser beam near the center of the cell. On the output side, a second 1 m focal length lens was used to collimate the Ramanshifted beam. All two-color measurements were carried out using spatially overlapped, counter-propagating laser beams. Digital delay generators (Stanford Research Systems, DG 535) were used to synchronize the light pulses.

PIE curves were recorded with the first laser set to populate an excited state of LiBe. The wavelength of the second laser was then swept to locate the onset of ionization. These measurements were conducted with the ionization zone located between the charged electrodes of the mass spectrometer. The local electric field of 364 V cm⁻¹ caused a depression of the IE by 115 cm⁻¹. PFI-ZEKE spectra for LiBe⁺ were recorded with sequential laser excitation occurring under nominally field-free conditions. Sequential excitation to long-lived Rydberg states was followed by the application of a 1.4 V cm⁻¹ pulse to induce field ionization and acceleration of the electrons to a microchannel plate detector. The delay between the laser excitation and ionizing field pulses was 2 μ s.

■ RESULTS AND ANALYSIS

LiBe 2² Π –**X**² Σ ⁺. RE2PI and LIF detection of the previously observed 2² Π –**X**² Σ ⁺ transition¹ was used in the process of optimizing LiBe production. Laser ablation of a freshly Li-coated Be rod initially produced Li_n clusters. After about 2 h of ablation at a pulse repetition rate of 10 Hz, workable number densities of LiBe were obtained. The 2² Π –**X**² Σ ⁺ bands were observed for the upper-state levels (ν' = 0–4), and the results were in good agreement with those reported by Schlachta et al.¹ The fluorescence decay lifetime of the 2² Π state had not been reported previously. In the present study, we examined the lifetime using the excitation of the 2–0 band. The resulting decay curve was well represented by a single-exponential decay with a lifetime of 38.4(5) ns.

DLIF spectra were recorded to characterize the ground-state vibrational levels. Figure 1 shows a DLIF spectrum that was

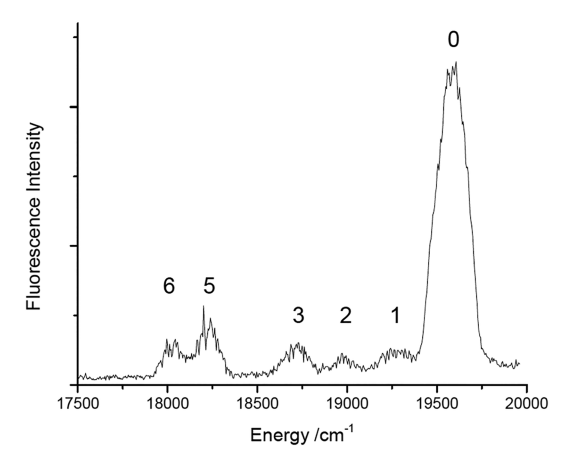


Figure 1. DLIF spectrum obtained using excitation of the $2^2\Pi - X^2\Sigma^+$ 2–0 band. The numbering above the peaks gives the ground-state vibrational assignments.

recorded using excitation of the 2-0 band. Note that the intensity of the resonant fluorescence signal was artificially high due to the contribution of scattered laser light. The intensity contours for the nonresonant bands were consistent with the upper-state vibrational numbering established by Schlachta et al. This assertion was based on Franck-Condon factors calculated using the point-wise potential energy curves that were reported by Fischer et al.²⁵ Band centers for the DLIF features were obtained by fitting a Gaussian line shape function to the peaks (the energies relative to $X^2\Sigma^+$, v''=0 are given in

Table 1. Relative Vibrational Energies of the Ground States of LiBe and LiBe+

ν	$E(LiBe(X))^a$	$E(LiBe^+(X))^a$	
0	0	0	
1	314	308.5	
2	592	612.9	
3	868	905.3	
4	1102	1190.9	
5	1357	1462.2	
6	1554		
7		2019.9	
8		2280.6	
_	. 1		

^aEnergies are in units of cm⁻¹.

Table 1). The line centers for v'' = 0-6 were fitted using the Morse energy-level expression

$$E(\nu) = \omega_{\rm e} \left(\nu + \frac{1}{2}\right) - \omega_{\rm e} x_{\rm e} \left(\nu + \frac{1}{2}\right)^2 \tag{1}$$

yielding vibrational constants of $\omega_e = 326.2(44)$ and $\omega_e x_e =$ 9.5(7) cm⁻¹ (with a standard deviation of 9 cm⁻¹). The highest vibrational level observed established a lower bound for the ground-state dissociation energy of $D_0 > 1554$ cm⁻¹, while extrapolation of the Morse vibrational constants gave an estimate for D_a of 2794(143) cm⁻¹.

LiBe 3 $^{2}\Sigma^{+}$ – $X^{2}\Sigma^{+}$. The theoretical calculations of Marino et al. were used to guide the search for bands of the $3^2\Sigma^+-X^2\Sigma^+$ transition. Our initial observations were made using resonanceenhanced one-color, two-photon ionization. Spectra with improved resolution were then obtained by switching to the LIF technique, where power broadening could be reduced. The origin band for this transition was found at 22 195.4 cm⁻¹ in reasonably good agreement with the computational prediction of 21 823 cm⁻¹. Figure 2 shows the 2-0 band as an example. As predicted by the calculations, the band was strongly red-shaded as the equilibrium internuclear distance for the $3^2\Sigma^+$ state is significantly larger than that of the ground state (calculated R_e values of 3.56 and 2.62 Å, respectively). The rotational structure was composed of just P- and R-branch lines, confirming the $3^2\Sigma^+$ symmetry of the upper electronic state. As only low-N rotational levels were observed, the simple rigid-rotor energy-level expression

$$\nu = T_{v',0} + B_v'N'(N'+1) - B_0''N''(N''+1)$$
(2)

was sufficient to fit the energy levels. In this expression, $T_{\nu',0}$ is the band origin and N is the Hund's case (b) integer quantum number for rotational motion. The spin-rotation splittings were below the instrumental resolution. Fitting was carried out using the PGOPHER software package²⁶ that, in addition to

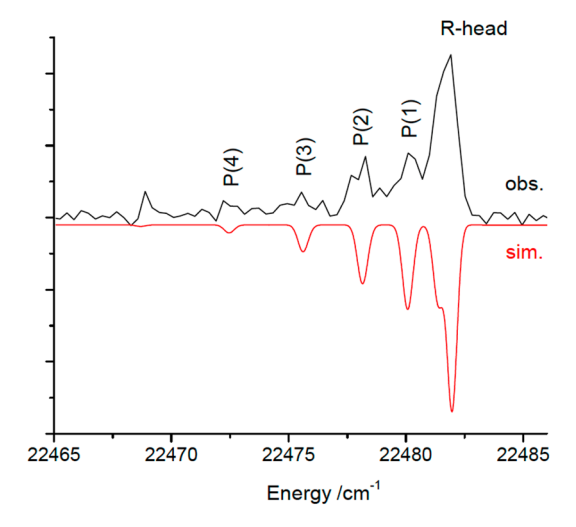


Figure 2. Rotational structure of the $3^2\Sigma^+ - X^2\Sigma^+$ 2–0 band recorded using the LIF technique. The P-branch lines are specified in terms of the Hund's case b rotational angular momentum quantum number. The downward-going trace is a simulation generated using the PGOPHER program. This simulation assumes a rotational temperature of 5 K.

fitting the energy levels, treats the line shape and line overlaps of the incompletely resolved spectrum. The downward-going trace in Figure 2 is a simulation generated using PGOPHER. For this simulation, the ground-state rotational constant was held at the value obtained by Schlachta et al. $(B_0'' = 0.637)$ cm⁻¹), and the spin-rotation interaction parameters for both the ground and excited states were fixed at 0 cm⁻¹. Because of the low rotational temperature (approximately 5 K), only the first few rotational levels contribute to the spectrum. Consequently, the fitting errors for the upper-state rotational constant were large, and we can only assert that the spectra were consistent with the simulations calculated using the molecular constants of Marino et al.

A simple vibrational progression was observed for the $3^2\Sigma^+$ $X^2\Sigma^+$ transition, corresponding to promotions from the ground-state v'' = 0 level to the v' = 0-7 levels of the upper state. The band heads for these transitions are listed in Table 2.

Table 2. Band Heads for the $3^2\Sigma^+-X^2\Sigma^+$ Transition of LiBe^a

	u'	$ u_0/\mathrm{cm}^{-1}$
	0	22 196.1
	1	22 339.3
	2	22 481.8
	3	22 623.3
	4	22 763.2
	5	22 900.5
	6	23 035.7
	7	23 167.0
_	•	

^aEnergies are in units of cm⁻¹.

Assuming that the upper-state rotational constants were close to 0.33 cm⁻¹, the band origins would be approximately 0.8 cm⁻¹ below the band heads. The vibrational structure of the $3^2\Sigma^+$ state was reasonably well fit using the Morse expression (eq 1), providing vibrational constants of $\omega_e = 146.9(3)$ and $\omega_e x_e = 0.99(6) \text{ cm}^{-1}$ (with a standard deviation of 0.4 cm⁻¹). The fluorescence decay lifetime of the $3^2\Sigma^+$ state, determined using excitation of the $\nu'=3$ level, was 51.0(4) ns.

LiBe 2 $^2\Sigma^+$ –**X** $^2\Sigma^+$. Theoretical calculations for the 2 $^2\Sigma^+$ –**X** $^2\Sigma^+$ band system 1,7,14,25 indicated that the origin should be found near 9780 cm $^{-1}$. Detection of the 2 $^2\Sigma^+$ –**X** $^2\Sigma^+$ transition was accomplished using two-color RE2PI with the ionization pulse following the excitation pulse with a delay of approximately 10 ns. The wavelength of the ionization laser was set to 280 nm. Figure 3 shows the 0–0 band. This trace

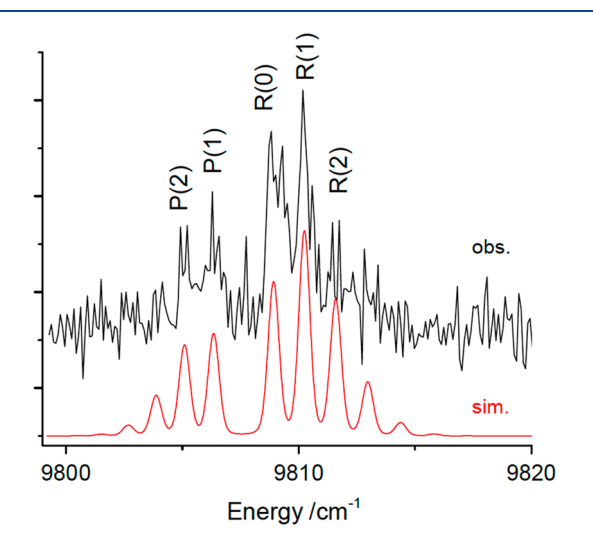


Figure 3. Rotational structure of the $2^2\Sigma^+-X^2\Sigma^+$ 0–0 band recorded using the RE2PI technique. The P- and R-branch lines are specified in terms of the Hund's case b rotational angular momentum quantum number. The lower trace (red) is a simulation generated using the PGOPHER program. This simulation assumes a rotational temperature of 4.5 K.

was taken with the laser line width reduced to 0.06 cm⁻¹, but the effective line width was determined by the trade-off between signal strength and power broadening. Despite the poor signal-to-noise ratio, several scans over this band confirmed a simple P- and R-branch rotational structure and established the band origin at 9807.5(2) cm⁻¹. The simulation in Figure 3 was carried out with the ground-state rotational constant fixed at 0.637 cm⁻¹, the upper-state rotational constant at $B_0' = 0.65$ cm⁻¹, and the rotational temperature set to 4.5 K. Because of the small number of rotational lines and the low signal-to-noise ratio, we estimate the error range for the upper-state rotational constant to be ± 0.01 cm⁻¹. Scanning to higher energy, the 2-0 band was found (at the lower resolution) with a band origin at 10 481(2) cm⁻¹. The intensity of this feature was approximately 1/10 of the intensity of the 0-0 band (vibrational assignment based on the theoretical predictions for the $2^{2}\Sigma^{+}$ vibrational constants^{1,7,14,25}). The 1-0 band could not be observed, indicating that its intensity was below the noise level. Similarly, a search for bands with v' > 2 did not yield any observable signals. The spontaneous decay lifetime of the $2^2\Sigma^+$, $\nu'=0$ level was examined by sweeping the delay between the excitation and ionization laser pulses. An exponential decay of the LiBe⁺ ion signal was observed that defined a lifetime of 60 ± 20 ns.

Near-UV Bands of LiBe and Dispersed Fluorescence Observation of the 1²II State. In our recent study of LiMg, band systems in the near-UV spectral range were examined using RE2PI, LIF, and DLIF techniques.²² The DLIF spectra

provided a means for observing the low-energy $1^2\Pi$ state. To facilitate similar measurements for LiBe, we examined excitation spectra occurring in the 29 000–31 750 cm⁻¹ range. Ten bands were observed in this region, but the signal-to-noise ratio was not sufficient to obtain rotationally resolved data. Band heads were found at 29 270, 29 295, 29 395, 29 499, 29 547, 29 814, 30 035, 30 111, 30 262, and 30 354 cm⁻¹. A spectrum showing these features is provided in the Supporting Information. The lifetime of the upper state of the 29 270 cm⁻¹ band was 38 ns, which was typical for emission from the near-UV excited states.

DLIF spectra were recorded for the more intense transitions. Figure 4 shows an example, obtained by exciting the band at

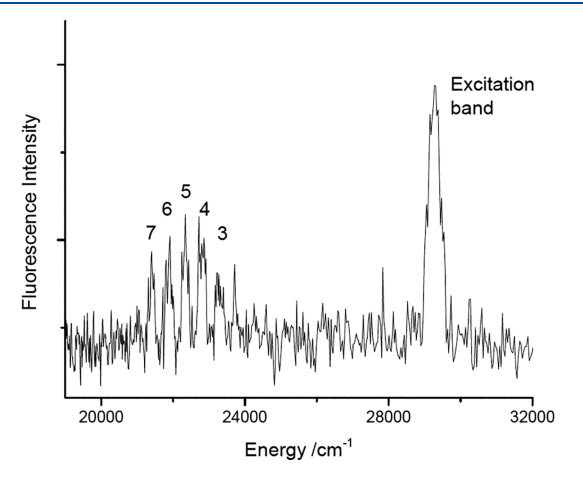


Figure 4. DLIF spectrum obtained using excitation of the 29 270 cm⁻¹ band. The peaks observed in the 21 000–24 000 cm⁻¹ range are assigned to the $4^2\Pi(3d)-1^2\Pi$ transition. The lower-state vibrational numbering is indicated above the peaks.

 $29\,270~{\rm cm}^{-1}$. This consists of resonant emission back down to the ground state and a vibrational progression to a lower-energy excited state that has an intensity maximum near 22 350 cm $^{-1}$.

Determination of the Ionization Energy of LiBe and the Vibrational Energy Levels of LiBe⁺ $X^{1}\Sigma^{+}$. Boldyrev et al. predicted an IE for LiBe of 40 569 cm⁻¹. The IE can also be estimated via the equation $IE(LiBe) = IE(Li) - D_0^+ + D_0$, where IE(Li) is the accurately known IE of atomic Li $(43\ 487.11\ \text{cm}^{-1})^{27}\ D_0^+$ is the dissociation energy for LiBe⁺ $(Li^+(1s^2) + Be(2s^2)$ asymptote), and D_0 is the dissociation energy of LiBe (Li(2s) + Be(2s 2) asymptote). The latter are available from published computational studies. For example, the results from Marino et al. vield an IE for LiBe of 40 995 cm⁻¹. The initial search for the ionization threshold of LiBe was carried out using the first laser pulse to excite the band head of the $2^2\Pi - X^{\bar{2}}\Sigma^+$ 2-0 band. The wavelength of the second laser was scanned over the expected energy range for two-color ionization. The threshold was found at 41 154(20) cm⁻¹, after correcting for the effect of the static electric field in the mass spectrometer. A second measurement, performed using the initial excitation of the $2^2\Pi - X^2\Sigma^+$ 3–0 band, provided an IE of 41 155(20) cm⁻¹. Switching to the more accurate PFI-ZEKE method, Figure 5 shows the feature produced by ionizing to the $v^+ = 0$ level of LiBe⁺ using the neutral molecule intermediate level $2^2\Pi \nu' = 2$. Because the rotational structure was not resolved, we have used the band center at a total energy of 41 146(5) cm⁻¹ to define the IE.

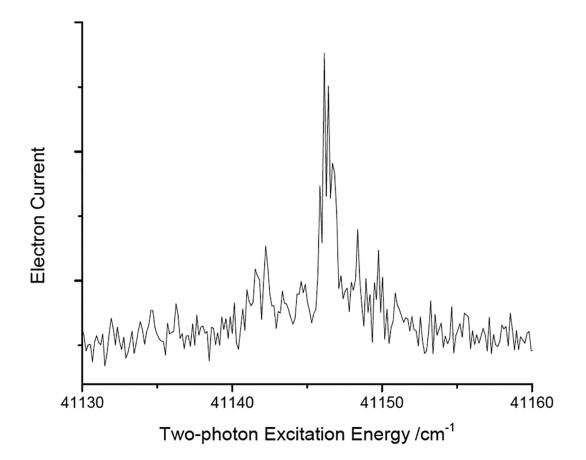


Figure 5. PFI-ZEKE spectrum showing the origin band for the two-photon ionization of LiBe (LiBe $X^2\Sigma^+$, $\nu''=0 \rightarrow \text{LiBe}^+ X^1\Sigma^+$, $\nu^+=0$). The first laser was set to excite the $2^2\Pi - X^2\Sigma^+$ 2–0 band.

Higher vibrational levels of LiBe⁺ $X^1\Sigma^+$ were detected using excitation via the $3^2\Sigma^+$ state because the longer equilibrium bond length for this state yielded better vibrational overlap with excited levels of the ion. By this means, we were able to observe vibrational levels spanning the $v^+=0$ to 8 range. The only break in this series was for $v^+=6$, where we could not find conditions that yielded workable signals. The energies of the observed levels, relative to the zero point of the ion, are listed in Table 1. Fitting eq 1 to these energies yielded vibrational constants of $\omega_e^+=313.3(16)$ and $\omega_e x_e^+=3.1(2)$ cm⁻¹, with a standard deviation for the fit of 5.3 cm⁻¹.

DISCUSSION

The vibrational constants for the ground states of LiBe and LiBe⁺ validate the results predicted using high-level computational methods. Table 3 lists the observed constants and a range of theoretical results. To minimize the errors introduced by imposing the Morse model on the data, it is most

Table 3. Ground-State Molecular Constants of LiBe and $LiBe^{+a}$

	ω_{e}	$\omega_{\mathrm{e}}\mathrm{x}_{\mathrm{e}}$	$\Delta G_{1/2}$	$D_{\rm e}$	source
LiBe					
	326.2(44)	9.5(7)	307.2(46)	>1715	exp, present work
			295		exp, ref 1
	302	9.5	283	2500	calc., ref 25
	300			2340	calc., ref 8
	298	9.8	278	2020	calc., ref 7
	354			2135	calc., ref 9
	340		299.5	2407	calc., ref 12
	307	1.9	303	2405	calc., ref 14
LiBe ⁺					
	313.3(16)	3.1(2)	305.9(17)	>2440	exp, present work
	311	4.8	301	4520	calc., ref 7
	320			4620	calc., ref 9
	318.4	4.31	310	4904	calc., ref 28
	323.7	5.45	313	4862	calc., ref 18
	324	4.87	314	4900	calc., ref 20

^aEnergies are in units of cm⁻¹.

appropriate to compare the measured and calculated values for $\Delta G_{1/2}.$ For the neutral molecule, most of the $\Delta G_{1/2}$ predictions agree with the measured value, to within the 1σ experimental error range. Even closer agreement is observed for LiBe+, where theoretical models are simplified by the fact that this is a closed-shell ion.

The ground-state bond energies are, of course, important properties. As the ionization of LiBe removes an electron from an antibonding orbital, it is reasonable to expect that the bond strength of LiBe+ would be appreciably greater than that of LiBe. As can be seen from the data listed in Table 3, this is borne out by the theoretical predictions. The bond dissociation energy of the ion appears to be about twice that of the neutral molecule. Our measurement for the IE of LiBe confirms the greater well depth for the ion. The relationship IE(Li) – $IE(LiBe) = D_0^+ - D_0$ shows that the difference in bond dissociation energies is 2341(5) cm⁻¹. The ground-state vibrational progressions observed in this study provide only lower limits for the bond dissociation energies. Extrapolation of the Morse vibrational constants for LiBe yielded an estimate for D_e of 2794(143) cm⁻¹, which is in reasonable agreement with the calculated values. However, this is probably fortuitous. The error range given here for the extrapolation is based on the error ranges of the fitted vibrational constants. If the true potential energy curve deviates from the Morse model at long range (which is likely), the errors could be considerably larger. We note that extrapolation of the vibrational structure for $LiBe^+$ to the dissociation limit using the Morse model gives D_e^+ = 7797(452) cm⁻¹, which is inconsistent with the theoretical predictions and the above analysis of the LiBe ionization

Another point of interest is the effect that ionization has on the equilibrium bond length and the vibrational constants. Theoretical calculations indicate a rather small change in the bond length on ionization. For example, You et al. ¹⁴ reported $R_{\rm e}$ values of 2.579 and 2.600 Å for LiBe and LiBe⁺, respectively. Surprisingly, the calculations yield a slightly longer bond length for the more deeply bound ion. Both the experimental data and the calculations show that the change in the harmonic vibrational constant is small. Consequently, the large difference in the bond dissociation energies arises from the smaller anharmonic vibrational constant of the ion.

DLIF spectra recorded using the excitation of the near-UV band at 29 270 cm⁻¹ exhibited emission back to a low-energy electronically excited state. The average spacing between the vibrational bands was 467(11) cm⁻¹. The intensity envelope indicates emission from a v' = 0 upper state, between states that have quite a large difference in their equilibrium distances. Because of this circumstance, we could not assume that the highest-energy discernible band in Figure 4 (23 306 cm⁻¹) was the origin band. (The sharp feature at 23 714 cm⁻¹ has a line width that was below that of the instrumental resolution and was therefore discounted as being mostly noise.) Fortunately, the low-energy electronic states are well separated with very different vibrational constants. On the basis of the results from published theoretical calculations, the lower state can be unambiguously assigned as $1^2\Pi$. The predicted T_e values for $1^{2}\Pi$ are 5000, 25 4768 and 4428 cm⁻¹. The transition at 22 306 cm⁻¹ in Figure 4 terminates on a level that is 5964 cm⁻¹ above the ground-state zero-point energy. The term energies and vibrational constants from refs 7, 14, and 25 are consistent in predicting that the 23 306 cm⁻¹ band terminates on the v'' = 3 level, establishing the vibrational numbering shown in Figure 4. The vibrational constants of You et al. ¹⁴ ($\omega_{\rm e} = 507.5$ and $\omega_{\rm e}x_{\rm e} = 3.36~{\rm cm}^{-1}$) yield an average value for the vibrational spacing of 470 cm⁻¹ for the v'' = 3-7 levels, in agreement with the experimental result. Using their vibrational energies to extrapolate the experimental data back to v'' = 0 yields a $1^2\Pi$ term energy of $T_0 = 4483~{\rm cm}^{-1}$.

An assignment for the upper state of the 29 270 cm⁻¹ band can be advanced on the basis of the calculations of Marino et al. This is the only published study that reports potential energy curves for the higher-energy states. Among these states there is a clear best fit with the observed data. The $4^2\Pi(3d)$ state was found to have a term energy of $T_e = 29 \, 113 \, \text{cm}^{-1}$ and an equilibrium bond length of 2.96 Å. (Marino et al.⁷ added the atomic orbital designation for the higher-energy states to emphasize their Rydberg character.) This state is unique in having a bond length that is long enough to account for the observed Franck-Condon intensity distribution. In fact, the predicted R_e is so large that the calculated intensity distribution peaks at v'' = 8, whereas the highest intensity in the observed spectrum was for v'' = 5. Reducing the R_e to 2.8 Å produced a Franck-Condon intensity distribution that was consistent with the DLIF spectrum. An inspection of the potential energy curves presented in Figure 2 of ref 7 indicates that there could be considerable latitude for the R_e value of $4^2\Pi(3d)$. The anomalously large R_e arises from an avoided crossing with the $3^2\Pi(3p)$ state that flattens out the $4^2\Pi(3d)$ potential energy curve near the minimum. Small errors in the details of this avoided crossing could readily account for the overestimation of the $4^2\Pi(3d)$ state R_e value without significantly compromising the agreement with T_e .

Returning to the lower energy range, the properties of the $2^2\Sigma^+$ state are of particular interest as You et al. 14 proposed that the $2^2\Sigma^+-X^2\Sigma^+$ transition is sufficiently diagonal to be used for laser cooling. In as far as we have been able to probe the $2^2\Sigma^+$ state, our spectroscopic data validate the theoretical calculations used to make the case for laser cooling. The measured T_0 value of 9807.6(2) cm⁻¹ is very close to the computed value of 9799 cm⁻¹, and the rotational structure of the origin band can be modeled using small differences between the upper- and lower-state rotational constants. Rotational structure modeling, detection of the weak 2-0 band, and the absence of the 1-0 band indicate that the bond length for $2^2\Sigma^+$ is slightly shorter than that of the ground state, in agreement with the calculations of Fischer et al.²⁵ and Marino et al. The measured interval between the v' = 2 and 0 levels of 674(2) cm⁻¹ was in agreement with the intervals predicted using the vibrational constants of Fischer et al.²⁵ (672 cm⁻¹), Marino et al. (678 cm⁻¹), and You et al. (678 cm⁻¹). Fischer et al.²⁵ and You et al.¹⁴ calculated the radiative decay lifetimes for the first few vibrational levels of the $2^2\Sigma^+$ state. For v' = 0, they obtained values of 78 and 75 ns, respectively. The present measurement gives a value of 60(20)ns, where the large error bars reflect the poor signal-to-noise ratio of the pump-probe measurements. We note that the predicted lifetime is within the 1σ error range. In considering the prospects for laser cooling, population loss via the $2^2\Sigma^+$ $1^2\Pi$ transition must be considered. Fischer et al. 25 found that the transition probability for this channel was a factor of 10³ smaller than that of the $2^2\Sigma^+$ - $X^2\Sigma^+$ transition, which would be manageable in a laser-cooling scheme. You et al. 14 concluded that the $2^2\Sigma^+$ – $1^2\Pi$ relaxation channel would not be problematic based on a Franck-Condon factor argument. They did not report a transition moment for this process.

The radiative lifetime was the only new data obtained for the $2^2\Pi$ state. Fischer et al.²⁵ predicted lifetimes for the $\nu'=0-3$ vibrational levels. Their results were almost independent of ν' , and their value for $\nu'=2$ of 38 ns was in excellent agreement with the measured value of 38.4(5) ns.

The $3^2\Sigma^+$ - $X^2\Sigma^+$ transition was observed for the first time. As noted above, the energy of the origin band for this transition was close to the theoretical prediction, and the rotational structure was consistent with a large equilibrium distance for the excited state. A potential energy curve for the $3^2\Sigma^+$ state is presented in Figures 1 and 2 of Marino et al., where the state is labeled as $D^2\Sigma^+$. It has a predicted well depth of 0.3 eV, an equilibrium distance of 3.56 Å, and an unusual shape. On page 3760 of their paper, Marino et al. 7 note that the shape of the $D^2\Sigma^+$ potential is influenced by an avoided crossing with the $^{2}\Sigma^{+}(3s)$ state. An inspection of Figure 2 in ref 7 indicates that the crossing of the diabatic potential energy curves would be found near 2.8 Å. Vertical excitation transitions would be expected to probe the region of the $3^2\Sigma^+$ potential energy curve that is most strongly perturbed by the state mixing. Consequently, it was somewhat surprising to find that the vibrational energy levels for v' = 0-7 were well represented by the Morse energy level expression. The vibrational constants from this fit, $\omega_{\rm e} = 146.9(3)$ and $\omega_{\rm e} x_{\rm e} = 0.99(6) \, {\rm cm}^{-1}$, were roughly consistent with the theoretical results (160 and 7.1 cm⁻¹), given that the definition of these parameters obtained from the theoretical results is in question due to the distorted shape of the potential energy curve.

In discussing the near-UV band used to observe emission to the $1^2\Pi$ state, we have proposed an assignment for the electronically excited state. Further assignment of the bands in this energy range has proven to be challenging using the data recorded to date. Because the 29 270 cm⁻¹ band was identified as the $4^2\Pi(3d)-X^2\Sigma^+$ origin, it is reasonable to search for higher vibrationally excited levels. Marino et al.7 provide vibrational constants of $\omega_e = 211$ and $\omega_e x_e = 3.1$ cm⁻¹, but given the perturbed character of the state, extrapolations based on these constants are dubious. The band at 29 499 cm⁻¹ could plausibly be the $\nu' = 1$ level, yielding a $\Delta G_{1/2}$ value of 227 cm⁻¹. There is no obvious candidate for the transition to v' = 2. The band at 29 814 cm⁻¹ is close to the energy predicted for the $6^2\Sigma^+(3d)$ state (29 805 cm⁻¹). This state shares the same Rydberg parentage as the $4^2\Pi(3d)$ state, so it is expected that both would be accessible from the ground state. Among the observed transitions, there are no good candidates for the $\nu' = 1$ level of $6^2\Sigma^+(3d)$. To make progress with the assignments for the higher-energy bands, future studies will need to achieve rotational resolution of the excitation bands and record better-quality DLIF spectra to facilitate vibrational assignments.

SUMMARY

Electronic spectra have been recorded for transitions from the $X^2\Sigma^+$ ground state of LiBe to the $2^2\Sigma^+$, $2^2\Pi$, and $3^2\Sigma^+$ states. Rotational resolution was achieved for several bands. Lower-resolution dispersed fluorescence spectra were used to characterize the vibrational levels of the $1^2\Pi$ and $X^2\Sigma^+$ states. Comparisons with the predictions from high-level electronic structure calculations show that multireference configuration interaction methods yield reliable results for the ground state and low-lying excited states of LiBe. The prediction by You et al. 14 that the $2^2\Sigma^+-X^2\Sigma^+$ transition would be suitable for laser cooling is supported by the experimental observations. Near-

UV band systems were examined, and the origin of the $4^2\Pi(3d)-X^2\Sigma^+$ transition was tentatively identified.

Two-photon ionization techniques were used to determine the IE of LiBe and the vibrational levels of the LiBe⁺ $X^1\Sigma^+$ ground state. Because ionization removes an electron from an antibonding orbital, an increase in the bond dissociation energy was both expected and observed. It was confirmed that the bond energy of LiBe⁺ is approximately twice that of LiBe. It is interesting that the theoretical calculations and measured molecular constants indicate little change in either the equilibrium distance or the harmonic vibrational frequency resulting from ionization.

ASSOCIATED CONTENT

Supporting Information

The Supporting Information is available free of charge at https://pubs.acs.org/doi/10.1021/acs.jpca.1c07014.

Time-resolved trace of fluorescence from the $2^2\Pi$ state and a separate trace of scattered laser light; corrected fluorescence decay curve obtained by subtraction of the laser scatter; a fitted exponential curve; low-resolution survey spectrum of the near-UV bands; and expanded view of the band at 30 262 cm⁻¹ (PDF)

AUTHOR INFORMATION

Corresponding Author

Michael C. Heaven — Department of Chemistry, Emory University, Atlanta, Georgia 30322, United States; orcid.org/0000-0003-4738-2408; Phone: (404) 727 6617; Email: mheaven@emory.edu

Authors

Thomas D. Persinger – Department of Chemistry, Emory University, Atlanta, Georgia 30322, United States Jiande Han – Department of Chemistry, Emory University, Atlanta, Georgia 30322, United States

Complete contact information is available at: https://pubs.acs.org/10.1021/acs.jpca.1c07014

Notes

The authors declare no competing financial interest.

ACKNOWLEDGMENTS

This work was supported by the National Science Foundation under grant CHE-1900555.

REFERENCES

- (1) Schlachta, R.; Fischer, I.; Rosmus, P.; Bondybey, V. E. The simplest heteronuclear metal cluster lithium-beryllium (LiBe). *Chem. Phys. Lett.* **1990**, *170* (5–6), 485–91.
- (2) Pewestorf, W.; Bonacic-Koutecky, V.; Koutecky, J. Ab initio configuration interaction study of mixed beryllium-lithium (BeLi_k) clusters (k = 1-9). *J. Chem. Phys.* **1988**, 89 (9), 5794–802.
- (3) Safonov, A. A.; Khrustov, V. F.; Stepanov, N. F. Calculation of potential curves of low-lying electron states of lithium beryllide and lithium-beryllium(1+) ion in a mixed orbital base by the SCF method. *J. Struct. Chem.* **1983**, 24 (2), 321–323.
- (4) Blustin, P. H.; Linnett, J. W. Applications of a simple molecular wave function. 6. FSGO [floating spherical Gaussian orbital] openshell calculations on first-row diatomic molecular systems. *J. Chem. Soc., Faraday Trans.* 2 **1974**, 70 (5), 826–36.

- (5) Jones, R. O. Molecular bonding in lithium-beryllium (LiBe), lithium-magnesium (LiMg), and lithium-calcium (LiCa). *J. Chem. Phys.* **1980**, 72 (5), 3197–200.
- (6) Pak, K.; Ermler, W. C.; Kern, C. W.; Bondybey, V. E. Full spin-orbit configuration interaction calculations on electronic states of lithium-beryllium (LiBe). *J. Cluster Sci.* **1991**, 2 (1), 19–28.
- (7) Marino, M. M.; Ermler, W. C.; Kern, C. W.; Bondybey, V. E. Spin-orbit configuration-interaction study of valence and Rydberg states of lithium-beryllium (LiBe). *J. Chem. Phys.* **1992**, *96* (5), 3756–66
- (8) Bauschlicher, C. W., Jr.; Langhoff, S. R.; Partridge, H. Theoretical study of the beryllium-lithium, beryllium-sodium, magnesium-lithium, magnesium-sodium, and aluminum-beryllium (BeLi, BeNa, MgLi, MgNa, and AlBe) molecules and their negative ions. *J. Chem. Phys.* **1992**, *96* (2), 1240–7.
- (9) Boldyrev, A. I.; Simons, J.; Schleyer, P. v. R. Ab initio study of the electronic structures of lithium containing diatomic molecules and ions. *J. Chem. Phys.* **1993**, *99* (11), 8793–504.
- (10) Begue, D.; Merawa, M.; Rerat, M.; Pouchan, C. Long-range coefficients for the low-lying electronic states of BeLi and Be₂. *J. Chem. Phys.* **1999**, *110* (4), 2051–2058.
- (11) Heaven, M. C.; Bondybey, V. E.; Merritt, J. M.; Kaledin, A. L. The unique bonding characteristics of beryllium and the Group IIA metals. *Chem. Phys. Lett.* **2011**, *506* (1–3), 1–14.
- (12) Kotochigova, S.; Petrov, A.; Linnik, M.; Klos, J.; Julienne, P. S. Ab initio properties of Li-group-II molecules for ultracold matter studies. *J. Chem. Phys.* **2011**, *135* (16), 164108.
- (13) Roostaei, B.; Ermler, W. C. Electric dipole transition moments and permanent dipole moments for spin-orbit configuration interaction wave functions. *Comput. Phys. Commun.* **2012**, *183* (3), 594–599.
- (14) You, Y.; Yang, C.-L.; Wang, M.-S.; Ma, X.-G.; Liu, W.-W. Theoretical investigation of the laser cooling of a LiBe molecule. *Phys. Rev. A: At., Mol., Opt. Phys.* **2015**, 92 (3-A), 032502.
- (15) Casals-Sainz, J. L.; Jimenez-Gravalos, F.; Costales, A.; Francisco, E.; Pendas, A. M. Beryllium Bonding in the Light of Modern Quantum Chemical Topology Tools. *J. Phys. Chem. A* **2018**, 122 (3), 849–858.
- (16) Pototschnig, J. V.; Hauser, A. W.; Ernst, W. E. Electric dipole moments and chemical bonding of diatomic alkali-alkaline earth molecules. *Phys. Chem. Chem. Phys.* **2016**, *18* (8), 5964–5973.
- (17) Fedorov, D. A.; Barnes, D. K.; Varganov, S. A. Ab initio calculations of spectroscopic constants and vibrational state lifetimes of diatomic alkali-alkaline-earth cations. *J. Chem. Phys.* **2017**, *147* (12), 124304.
- (18) Ghanmi, C.; Farjallah, M.; Berriche, H. Theoretical study of the alkaline-earth (LiBe)⁺ ion: structure, spectroscopy and dipole moments. *J. Phys. B: At., Mol. Opt. Phys.* **2017**, *50* (5), 055101.
- (19) Rakshit, A.; Deb, B. Formation of cold molecular ions by radiative processes in cold ion-atom collisions. *Phys. Rev. A: At., Mol., Opt. Phys.* **2011**, 83 (2), 022703.
- (20) Bala, R.; Nataraj, H. S.; Abe, M.; Kajita, M. Accurate ab initio calculations of spectroscopic constants and properties of BeLi⁺. *J. Mol. Spectrosc.* **2018**, 349, 1–9.
- (21) Barry, J. F.; Shuman, E. S.; Norrgard, E. B.; DeMille, D. Laser radiation pressure slowing of a molecular beam. *Phys. Rev. Lett.* **2012**, *108* (10), 103002.
- (22) Persinger, T. D.; Han, J.; Heaven, M. C. Electronic Spectroscopy and Photoionization of LiMg. *J. Phys. Chem. A* **2021**, 125 (17), 3653–3663.
- (23) Duncan, M. A. Laser vaporization cluster sources. Rev. Sci. Instrum. 2012, 83 (4), 041101.
- (24) Heaven, M. C. Probing actinide electronic structure using fluorescence and multi-photon ionization spectroscopy. *Phys. Chem. Chem. Phys.* **2006**, 8 (39), 4497–4509.
- (25) Fischer, I.; Bondybey, V. E.; Rosmus, P.; Werner, H. J. Theoretical study of the electronic states of beryllium lithium and beryllium dimer ion(1+). *Chem. Phys.* **1991**, *151* (3), 295–308.

- (26) Western, C. M. PGOPHER: A program for simulating rotational, vibrational and electronic spectra. *J. Quant. Spectrosc. Radiat. Transfer* **2017**, *186*, 221–242.
- (27) NIST Atomic Spectra Database; National Institute of Standards and Technology: Gaithersburg, MD, 2021. https://physics.nist.gov/asd.
- (28) You, Y.; Yang, C.-L.; Wang, M.-S.; Ma, X.-G.; Liu, W.-W. An ab initio study of the ground and low-lying excited states of LiBe⁺. *J. At. Mol. Sci.* **2018**, *6* (2), 63–71.